IEEE Access
Multidisciplinary | Rapid Review | Open Access Journal

Received December 28, 2020, accepted January 17, 2021, date of publication January 20, 2021, date of current version January 27, 2021.

Digital Object Identifier 10.1109/ACCESS.2021.3053116

Time-Domain Scattering Characteristics and Jamming Effectiveness in Corner Reflectors

YING LUO, LIXIN GUO, (Senior Member, IEEE), YANCHUN ZUO, AND WEI LIU, (Member, IEEE)
School of Physics and Optoelectronic Engineering, Xidian University, Xi'an 710071, China

Corresponding author: Lixin Guo (lxguo@xidian.edu.cn)

This work was supported in part by the National Natural Science Foundation of China under Grant 61871457, and in part by the Foundation for Innovative Research Groups of the National Natural Science Foundation of China under Grant 61621005.

ABSTRACT The outboard corner reflectors are widely used as a countermeasure to radar tracking and detection. Therefore, it is essential to determine the composite time-domain scattering characteristics of the corner reflector and ship against the sea background and the jamming effectiveness of the corner reflector array. In this paper, the composite electromagnetic scattering characteristics of ship target, corner reflector, and the sea surface are studied based on the time-domain bouncing ray method (TDSBR). The radar echo and broadband radar cross section (RCS) results for the time domain pulse incident are also obtained and the high-resolution range profile (HRRP) is calculated. We then devise an evaluation system based on centroid jamming intensity and range profile similarity to determine the jamming characteristics of passive jamming. We further propose an array composing of three sizes of corner reflectors. Finally, the centroid jamming effectiveness is analyzed by comparing the RCS of the corner reflector array and the ship, and the deception jamming effectiveness is measured by calculating the range profile similarity based on the cosine similarity method and the range profile peak envelope overlap. Simulation results show that the reflector array can achieve a good performance both for centroid and range profile deception. The simulation results given and the evaluation method proposed in this paper provides significant practical insights into the design and analysis of the passive jamming systems.

INDEX TERMS Time-domain bouncing ray method, jamming effectiveness evaluation, passive jamming, high-resolution range profile.

I. INTRODUCTION

The corner reflector is a widely used passive jammer [1], [2], which is composed of several orthogonal metallic planes. The incident electromagnetic wave is easily reflected backward by these planes to produce a strong echo. The model of the trihedral corner reflector is shown in Fig. 1(a). Such reflectors are used to simulate stationary ground targets as shown in Fig. 2. This geometric unit can be used to form a polyhedral corner reflector [3] (see, Fig.1 (b)). The icosahedron triangular trihedral corner reflector (ITTCR) is also shown in Fig. 3 [4], which is widely used in the navy because of stable reflection performance in all observation directions due to its central symmetric geometric structure.

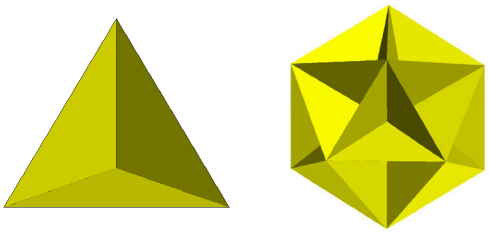

FIGURE 1. The model of corner reflectors. (a) trihedral corner reflector, and (b) icosahedron triangular trihedralcorner reflector.

Furthermore, the corner reflector and the ship are both targets with rigid structures [5]. For high resolution sensing the echoes and the range profiles of the ship and a single corner

The associate editor coordinating the review of this manuscript and approving it for publication was Mauro Fadda.

FIGURE 2. The array of corner reflector on the ground [3].

reflector are different. Hence, multiple corner reflectors can be used as a reasonable deployment to simulate the radially distributed scattering center of the ship, which provides high jamming efficiency [6].

In the existing research works, most scholars focus on the electromagnetic scattering characteristics of the target. Nevertheless, the scattering characteristics of passive jammers such as corner reflectors in the time domain and for tactical use have not been investigated. As an essential role in the future electromagnetic warfare, the corner reflector determines the jamming effectiveness and the survival rate of the equipment. Therefore, it is of great significance to analyze the electromagnetic scattering and jamming effectiveness of the corner reflector and the array.

Time-domain scattering analysis of electrically large-scale targets is often focused on enhancing the efficiency and accuracy of the numerical algorithms [7]. Some scholars also study the composite time-domain echo estimation method of a ship with a corner reflector using TDSBR [8]. This method is also used in this paper to provide the scattering data of the jamming efficiency analysis of the corner reflector array. For practical application scenarios, there exits composite scattering between sea surface and the target, it is necessary to consider not only the scattering of the target itself but also the multipath problem of scattering between the sea surface and the target.

In terms of the electromagnetic scattering results of the icosahedral corner reflector, some research works investigate the effect of the manufacturing errors of the corner reflector array on its RCS characteristics [9]. The RCS evaluation methods of the corner reflectors are also addressed in [10], [11]. Although these studies provide the relevant characteristics of the ITTCR structure and offer ideas for calculating of corner reflector scattering, they lack application-level analysis and calculations based on practical data. To study the jamming mechanism of decoy in a dynamic environment, [12] establishes the decoy signal model. Furthermore, the scattering and jamming principle of the corner reflector is studied based on the physical optics method [13], and the jamming mechanism in the naval battlefield environment is described [14]. Although there exists several academic research on the evaluation of the interference effect of HRRP on the corner reflector [15], the simulation results are based on electromagnetic calculation software. In such research works, the Euclidian distance comparison is used for calculating the similarity of the distance profile. This is, however, not suitable for the calculation of the similarity of the range profile. This is because the Euclidian distance is sensitive to the absolute values, and it may cause large errors in the similarity calculation due to factors such as peak staggering.

In this paper, we solve the problem of corner reflector scattering and jamming characteristics. The article is organized as follows. In Section I, the research status of scattering and jamming of corner reflector is reviewed. In Section II, the principle of the time-domain bouncing ray method, and acquisition method of range profile obtained from time-domain echo, and the similarity calculation method of range profile are described. In Section III, the correlation simulation calculations and jamming principle analysis are carried out to lay the foundation for the subsequent jamming effect evaluation. Finally, in Section IV, for the corner reflector array composed of three sizes, a comprehensive evaluation method is given from three dimensions: centroid interference, range profile cosine similarity, and range profile overlap ratio, based on which the evaluation results are obtained.

II. PRINCIPLES OF ELECTROMAGNETIC SCATTERING CALCULATION AND PROCESSING

This section describes the principle of the time-domain shooting and bouncing ray method for calculating scattered electric field. We further present the principle of obtaining range profile from time-domain echoes and the principle of similarity solution.

A. TDSBR METHOD

The calculation formulas of the TDSBR method are derived from the frequency domain bouncing ray (FDSBR) method [16]. These formulas are related by applying the inverse Fourier transform. The TDSBR algorithm mainly involves the time domain geometric optics (TDGO) and the time domain physical optics (TDPO) methods. The TDGO method is adopted to track and update the information that the ray takes, and the TDPO method is used to calculate the far-field excited by the induced current on the target surface.

Modulated Gaussian pulse is a common pulse incident wave that does not contain low-frequency components, hence, it does not produce singular values in the RCS calculation. The time-domain expression is

$$E(t) = \cos\left[2\pi f_0(t - t_0)\right] \exp\left[-4\pi \frac{(t - t_0)^2}{\tau^2}\right] \quad (1)$$

where the pulse frequency width is B which denotes the difference between the upper and lower limit frequencies, and the pulse width is $\tau = 2/B$, and $f_0 =$ central frequency.

For brevity of the derivations, in the subsequent programming, the first derivative function of modulated Gaussian pulse is set as the incident wave [17]. The expression of the incident wave is represented by $G(t)$, and the expression of

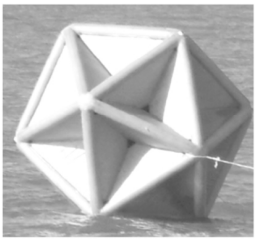

FIGURE 3. The icosahedron triangular trihedral corner reflector (ITTCR) [4].

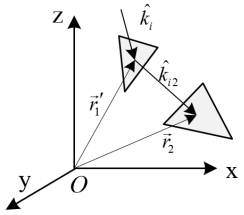

FIGURE 4. The position distribution of incident wave and facets.

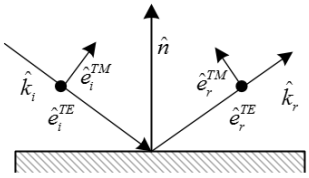

FIGURE 5. The decomposition of incident wave and reflected wave.

the electric field vector of the incident wave is

$$\vec{E}_i(\vec{r}',t)=\hat{e}_i G(t)*\delta\left(t-\frac{\hat{k}_i\cdot\vec{r}'}{c}\right)=\hat{e}_i G\left(t-\frac{\hat{k}_i\cdot\vec{r}'}{c}\right) \quad (2)$$

where the symbol $*$ represents convolution operation, $\hat{k}_i =$ direction of the incident wave, and $\vec{r}' =$ coordinates of the target panel, shown in Fig.4.

According to the TDGO method, the electric field scattered by the first surface facet is

$$\begin{aligned}\vec{E}_{r1}(\vec{r}',t)&=\vec{E}^{TE}_{r1}(\vec{r}',t)+\vec{E}^{TM}_{r1}(\vec{r}',t)\\&=R^{TE}\left[\vec{E}_i(\vec{r}',t)\cdot\hat{e}_i^{TE}\right]\hat{e}_i^{TE}\\&\quad+R^{TM}\left[\vec{E}_i(\vec{r}',t)\cdot\hat{e}_i^{TM}\right](\hat{e}_i^{TM}\times\hat{k}_s)\end{aligned} \quad (3)$$

where R^{TE} and R^{TM} are the reflective coefficients in the two polarization states, $\hat{e}_i^{TE}$ and $\hat{e}_i^{TM}$ are the wave vectors in the two polarization states, shown in Fig.5, and $\hat{k}_s$ is the direction of the field to be solved.

According to the law of reflection and considering the time delay, the incident electric field for the second facet is expressed as

$$\vec{E}_{i2}(\vec{r}',t)=\vec{E}_{r1}(\vec{r}',t)*\delta\left(t-\frac{\hat{k}_{i2}\cdot(\vec{r}_2'-\vec{r}'_1)}{c}\right)$$

$$\begin{aligned}&=G(t)\left[R^{TE}(\hat{e}_i\cdot\hat{e}_i^{TE})\hat{e}_i^{TE}\right.\\&\quad\left.+R^{TM}(\hat{e}_i\cdot\hat{e}_i^{TM})(\hat{e}_i^{TE}\times\hat{k}_s)\right]\\&\quad*\delta\left(t-\frac{\hat{k}_i\cdot\vec{r}_1'}{c}\right)*\delta\left(t-\frac{\hat{k}_{i2}\cdot(\vec{r}_2'-\vec{r}'_1)}{c}\right)\end{aligned} \quad (4)$$

The scattered field is obtained from (3), and the incident field after multiple scattering is obtained from (4) until the ray leaves the target.

The far-field excited by the equivalent surface element on each facet is also calculated using the PO theory and Stratton-Chu formula. Therefore, the electric field calculation formula in the time domain is obtained by performing an inverse Fourier transform of the frequency domain formula

$$\begin{aligned}&\vec{E}_s(\vec{r}',t)\\&=-\frac{1}{4\pi Rc}\vec{A}\int_s\partial\vec{E}_i\left(t-R/c-(\hat{k}_i-\hat{k}_s)\vec{r}'/c\right)\Big/\partial t d\mathrm{S}\end{aligned} \quad (5)$$

where R is the coordinate distance of the field point, and

$$\vec{A}=\hat{k}_s\times\left[\begin{array}{l}\hat{k}_s\times\left(\begin{array}{l}-(1-R^{TE})(\hat{n}\cdot\hat{k}_i)(\hat{e}_i\cdot\hat{e}_i^{TE})\hat{e}_i^{TE}\\+(1+R^{TM})(\hat{e}_i\cdot\hat{e}_i^{TM})(\hat{n}\times\hat{e}_i^{TE})\end{array}\right)\\-\left(\begin{array}{l}(1+R^{TE})(\hat{e}_i\cdot\hat{e}_i^{TE})(\hat{n}\times\hat{e}_i^{TE})\\+(1-R^{TM})(\hat{n}\cdot\hat{k}_i)(\hat{e}_i\cdot\hat{e}_i^{TM})\hat{e}_i^{TE}\end{array}\right)\end{array}\right] \quad (6)$$

Vector $\vec{A}$ is a symbol used to simplify the description, which represents the coupling between incident wave and scattered one. The integral in (4) is then rewritten as

$$\begin{aligned}&\int_s\frac{\partial\vec{E}_i\left(t-R/c-(\hat{k}_i-\hat{k}_s)\vec{r}'/c\right)}{\partial t}d\mathrm{S}\\&\qquad=\vec{E}_i(t)*\int_s\delta'\left(t-R/c-(\hat{k}_i-\hat{k}_s)\vec{r}'/c\right)d\mathrm{S}\end{aligned} \quad (7)$$

For the backscattering, $\hat{k}_s=-\hat{k}_i$, and the Green formula is used to convert the surface integral into a line integral expression. Suppose that $\vec{w}=\hat{k}_i-\hat{k}_s$, $\vec{\alpha}$ represents the projection vector of $\hat{k}_i-\hat{k}_s$ on the plane of the facet and

$$\vec{\alpha}=\left(\hat{k}_i-\hat{k}_s\right)-\left[\left(\hat{k}_i-\hat{k}_s\right)\cdot\hat{n}\right]\hat{n} \quad (8)$$

The above integral is then obtained using the following expression without area fraction, which can be divided into the following three cases

$$\begin{aligned}&\int\delta'\left(t-(\hat{k}_i-\hat{k}_s)\vec{r}'/c\right)d\mathrm{S}\\&=\begin{cases}\delta'\left(t-(\hat{k}_i-\hat{k}_s)\vec{r}'/c\right)\Delta S & \hat{k}_i\cdot\hat{n}=-1\\\dfrac{c}{\alpha^2}\displaystyle\sum_{i=0}^{3}(\vec{w}\times\hat{n})\\\quad\cdot(\vec{p}_{i+1}-\vec{p}_i)\begin{cases}\delta\left(t-\dfrac{\vec{w}\cdot\vec{p}_i}{c}\right) & \vec{w}\cdot\Delta\vec{p}_i=0\\\dfrac{c}{\vec{w}\cdot\Delta\vec{p}_i}\left[\begin{array}{l}\varepsilon\left(t-\frac{\vec{w}\cdot\vec{p}_i}{c}\right)\\-\varepsilon\left(t-\frac{\vec{w}\cdot\vec{p}_{i+1}}{c}\right)\end{array}\right] & \vec{w}\cdot\Delta\vec{p}_i\neq0\end{cases}\end{cases}\end{aligned} \quad (9)$$

The time-domain electric field integral formula (9) is then used to obtain the target scattering time-domain echo result under the incident of the time-domain pulse. We then obtain the ratio between the Fourier transform result of the echo and the Fourier transform result of the incident wave. The values of the RCS change within a certain bandwidth is then obtained as

$$\sigma = 4\pi \lim_{R\to\infty} R^2 \frac{|\vec{E}_s|^2}{|\vec{E}_i|^2} \tag{10}$$

B. PRINCIPLE OF HIGH-RESOLUTION RANGE PROFILE

Assume that the target is composed of N scattering points and x_i is the position coordinate of each scattering point. The scattering electric field of the target at different frequencies is the superposition of the scattering intensity of n scattering points, and the expression is:

$$E_s(f) = \sum_{i=1}^{N} E_{ri} \cdot \exp\left[-j2\pi(2f/c)x_i\right] \tag{11}$$

where E_{ri} is the backscattering electric field intensity of the i-th scattering point. Applying the Fourier transform, on the time-domain echo result obtained by the time-domain bouncing ray method, and calculating the ratio with the incident wave spectrum, the total scattering intensity, i.e., the electric field $E_s(f)$ can be then obtained.

Here we perform the inverse Fourier transform on the above formula to obtain the HRRP of the target:

$$\begin{aligned} E_s(x) &= F^{-1}\left[E_s(f)\right] \\ &= \sum_{i=1}^{N} E_{ri} \cdot \int_{f_1}^{f_2} \exp\left[-j2\pi(2f/c)(x-x_i)\right] d\left(\frac{2f}{c}\right) \end{aligned} \tag{12}$$

where the bandwidth is $B = f_2 - f_1$, and the central frequency is $f_0 = (f_1 + f_2)/2$.

Using the above, the range profile of the target can be indirectly obtained by obtaining the time-domain echo for the modulating Gaussian pulse incidence [18].

C. SIMILARITY SOLUTION METHOD

The similarity of the range profile in this paper refers to the closeness of the two sets of results produced by the ship and the corner reflector array. Using the Euclidean distance as a metric for similarity results in a small difference in the abscissa of the peak of the two sets of results. This then results in an extremely low similarity value. To address this issue, here we use the cosine similarity method.

The cosine similarity method is often used to calculate the similarity between the texts or users. The cosine similarity uses the cosine value of the angle between two vectors as a measure of the difference between two individuals. If the cosine value approaches 1, then the included angle tends to 0, indicating that the two vectors are more similar. If the cosine value becomes close to 0, then the included angle tends to 90 degrees, indicating that the two vectors are dissimilar.

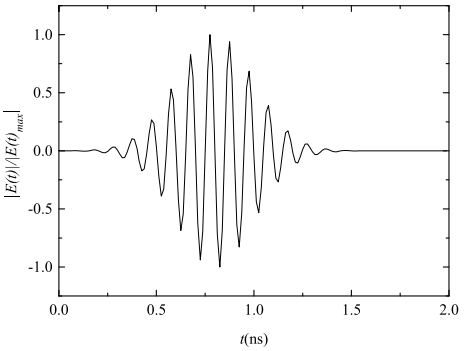

FIGURE 6. The time-domain pulse form of the incident wave.

After improvement, the similarity calculation formula of this article is obtained as

$$\begin{aligned} similarity &= \frac{\cos(\theta)+1}{2} \\ &= \frac{1}{2}\left[\frac{\sum_{i=1}^{n}(P_{1i}\times P_{2i})}{\sqrt{\sum_{i=1}^{n}(P_{1i})^2}\times\sqrt{\sum_{i=1}^{n}(P_{2i})^2}}+1\right] \end{aligned} \tag{13}$$

where P_{1i} and P_{2i} represent the normalized HRRPs of the ship and the corner reflector under a certain incident angle, respectively. The value range of (13) is (0, 1), which is consistent with the similarity definition in this paper.

III. SIMULATION CALCULATION AND ANALYSIS

In this section, the TDSBR method is used to calculate the composite time-domain echo and the RCS of the ship, the corner reflector and the sea surface, and the range profiles of the ship with multiple incident angles. Furthermore, the scattering characteristics of the ship, the array arrangement, and the jamming mechanism are analyzed.

A. COMPOSITE SCATTERING CHARACTERISTICS

The incident wave is set as the first derivative function of the modulated Gaussian pulse. The central frequency of the incident wave is $f_0 = 10$ GHz and the bandwidth, B, is 4 GHz. The normalized time-domain waveform and spectrum are obtained by simulation and presented in Figs. 6 and 7.

The TDSBR method is used to calculate the composite scattering characteristics of a 10:1 scaled ship. The prototype length of the ship is about 140 m, the sea measures 30 by 30 meters, the wind speed near the sea surface is 3 m/s, the wind direction angle is 0°, and the incident angle is $\theta = 30°, \varphi = 180°$.

The echo results are shown in Fig. 8. The corresponding RCSs of the ship and the ship with sea surface are also shown in Fig. 9. In Fig. 8, the scattering characteristics of the ship and the composite scattering characteristics of the ship and sea surface time-domain are shown. As it is seen there are small fluctuations with long-term effects in the echo originated from the scattering of the sea surface. It is further

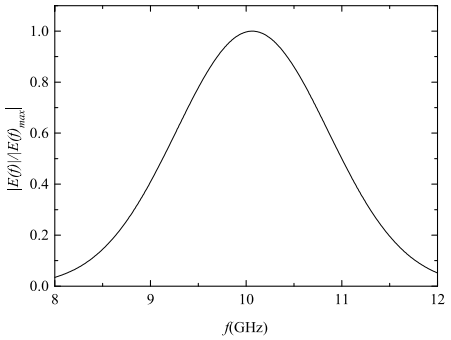

FIGURE 7. The frequency spectrum of the incident wave.

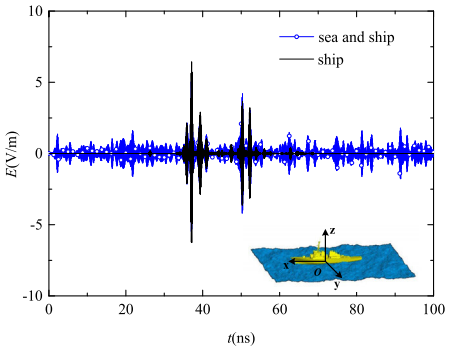

FIGURE 8. The composite scattering echo from sea and scaled ship.

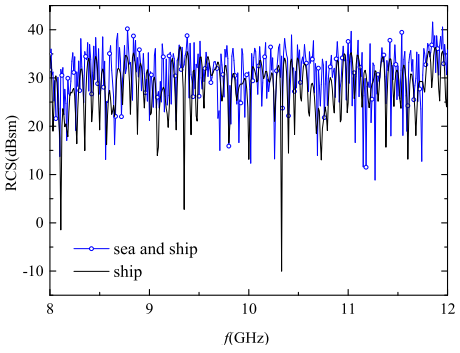

FIGURE 9. The frequency domain results of radar cross section (RCS).

seen that the peak position of the large fluctuations is the scattering of the ship itself or the composite scattering of the sea surrounding the ship. The corresponding broadband RCS comparison results are shown in Fig. 9, and as it is seen, the range of the overall RCS value depends on the scattering of the ship.

For a similar setting, in Figs. 11 and 12, we present the composite scattering of ICCTR with a diameter of 2 m and a sea surface of 30 by 30 meters. Fig. 10 shows that the time-domain echo peak of the corner reflector is larger than that of the oscillating sea surface echo and there is also a scattering center. It is further seen in Fig. 11 that the variation of RCS with frequency is smooth. Comparison with the results presented in Figs. 9 and 10 suggest that the echo of the corner

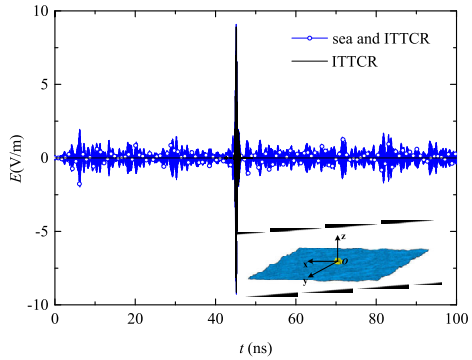

FIGURE 10. The composite scattering echo from sea and ITTCR.

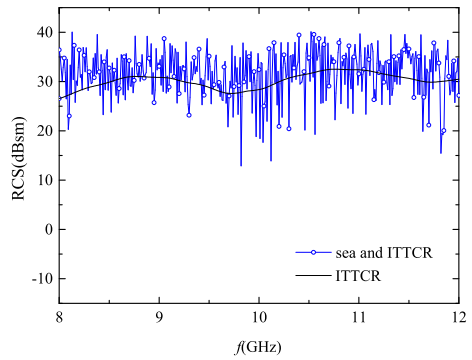

FIGURE 11. The frequency domain results of radar cross section (RCS).

reflector is similar to that of the ship, and the fluctuation of RCS with frequency is also close to that of the ship.

The simulation results show the effectiveness of the corner reflector as a passive jammer, nevertheless, how to increase its jamming effectiveness requires further investigations.

B. RANGE PROFILE CHARACTERISTICS

Using the scattering results calculated above, we can obtain the HRRP of the target. Our objective is to use the corner reflector array to simulate the scattering characteristics of the ship, and both of them were at sea when they were searched. Moreover, the sea clutter can be filtered by mature technology, so it is not necessary to consider the sea surface, which is removed in the subsequent simulation.

The central frequency of the incident wave is $f_0 = 10$ GHz, the bandwidth B is 1 GHz, and the incident angle is $\theta = 60°, \varphi = 0°$. The time-domain echo of a 140 m long ship is obtained by simulation (see, Fig. 12), and the corresponding HRRP is presented in Fig. 13. As it is seen the strong scattering points in the time-domain and the HRRP results of the target are at the same point.

In the following, we calculate the HRRP of the ship at different incident angles in $\theta = 60°$, and $\varphi = 0°$ to $\varphi = 180°$. Two-norm normalizations are carried out, as shown in Fig. 14. We cover a variety of situations, where the electromagnetic waves are incident from the front to the tail of the ship, which

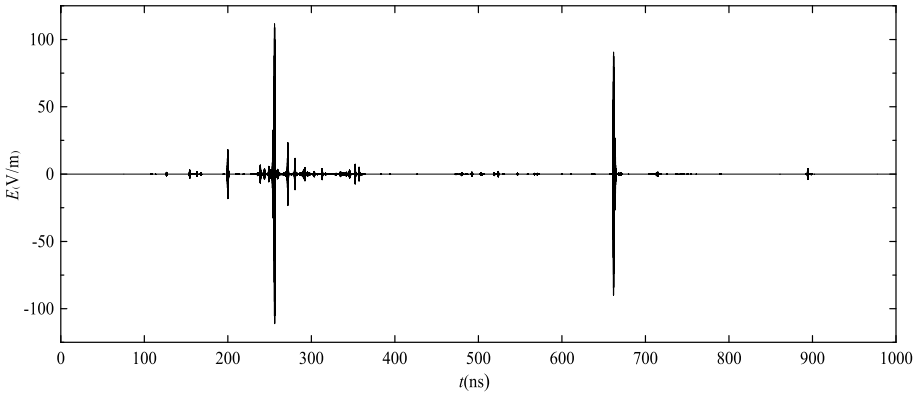

FIGURE 12. The time-domain scattered waves from ship.

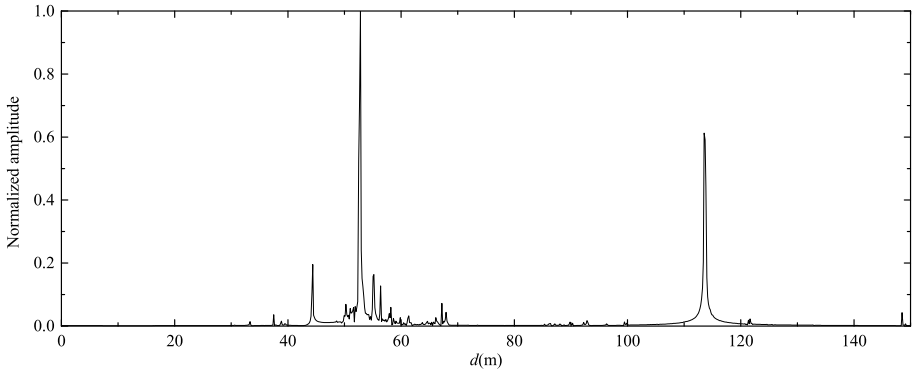

FIGURE 13. The high-resolution range profile of ship.

lays the foundation for the subsequent range profile similarity solution.

Fig. 14 shows that in the case of head-on or tail incidents, the range profile has a wide distribution range on the distance axis. In the case of the side incident, the range profile is concentrated within a short distance which is related to the longitudinal and lateral structure of the ship. This suggests that the linear arrangement of the corner reflector array which is parallel to the axial direction of the ship provides a higher jamming performance as it generates a more similar range profile with that of the ship compared with other released patterns.

C. JAMMING MECHANISM ANALYSIS

As a false target, the corner reflector needs to generate a radar cross-section comparable to that of a ship in order to achieve the purpose of centroid interference. Further, in terms of radar imaging, a range profile that is difficult to distinguish from the ship should also be generated by the corner reflector. Therefore, the evaluation of jamming effectiveness should proceed from two perspectives, radar cross section and high-resolution range profile [20].

1) RADAR CROSS SECTION

To ensure the performance of centroid interference, the RCS of the jammer should not be less than that of the ship. Here, according to the results of related research works, the corner reflector radius is set to 2 m.

For an incident zenith angle $\theta = 60°$, the RCS of a 140 m long ship versus the azimuth is presented in Fig. 15(a). The RCS of the ITTCR with a radius of 2 m is also shown in Fig. 15(b). The RCS results at three frequencies 9.5 GHz, 10 GHz, and 10.5 GHz are also shown in Fig. 15. It is seen that the RCS of the corner reflector is close to or greater than the RCS of the ship at each frequency point. It is further seen that the single corner reflector meets the requirements of centroid jamming. Furthermore, using a set of corner reflectors results in higher performance of the centroid jamming.

2) HIGH SOLUTION RANGE PROFILE

The relevant parameters of the corner reflector array need to be optimized, to enable the fabrication of a range profile that is similar to that of the ship. Fig. 16 shows the range profile of the ship with a zenith angle $\theta = 60°$ and head-on incidence. To obtain strong scattering points, we take the inverse logarithm of its longitudinal axis, and the corresponding relationship between the strong scattering points and the ship structures is obtained. We then investigate the range profile of the corner reflector. A single corner reflector can also produce a point-like target range profile as shown in Fig. 17(a). In making an array, considering multiple sizes of corner reflectors provides a better simulation of the ship's

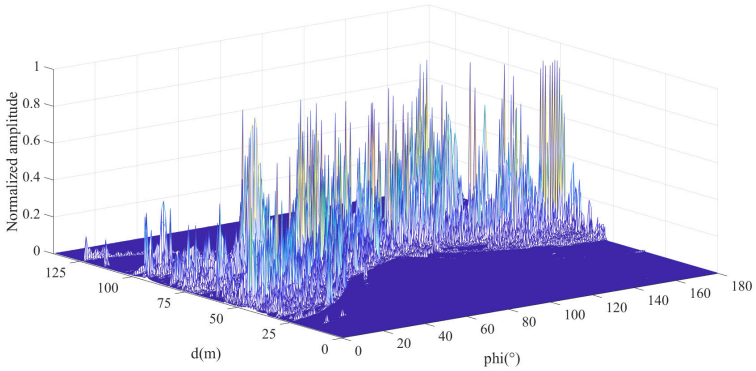

FIGURE 14. The high-resolution range profile of the ship at different incident azimuths.

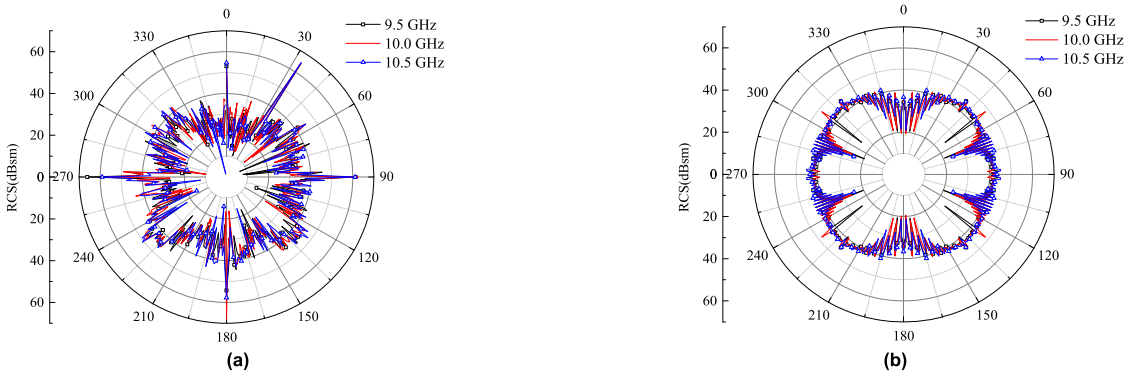

FIGURE 15. The results of radar cross section varying with azimuth, (a) ship and (b) ITTCR.

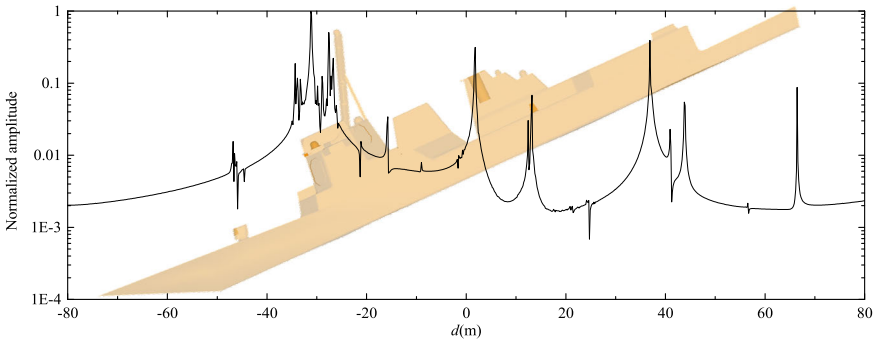

FIGURE 16. The range profile and strong scattering point distribution of ship.

high-resolution range profile characteristics. In Fig. 17(b) we present the high-resolution range profile results obtained by an array composed of corner reflectors with a radius of 1 m, 1.5 m, and 2 m, and the incident angle $\theta = 60°$, $\varphi = 0°$.

The above results suggest that compared with the single-size corner reflectors in the existing research works, multi-size corner reflector arrays provide better similarity.

IV. EVALUATION PROCESS

To evaluate the jamming effectiveness of the corner reflector array, the appropriate size a of corner reflectors should be selected, and the number of corner reflectors should be determined. The electromagnetic scattering characteristics and range profile are then calculated. Then, the RCS results of the array and the ship are compared, and the similarity of HRRP is solved. This provides a comprehensive evaluation of the jamming performance. The similarity of the distance profile is measured by the cosine similarity and the area of the envelope overlap. The block diagram of the steps for the jamming assessment is shown in Fig. 18.

In the previous works, the elevation angle of the incident wave is set as $\theta = 90°$ for calculating the HRRP results [19]. This situation however does not comply with the radar tracking of ships. To address this issue, in this paper, the simulation research is carried out for oblique incidence, i.e., $\theta = 60°$.

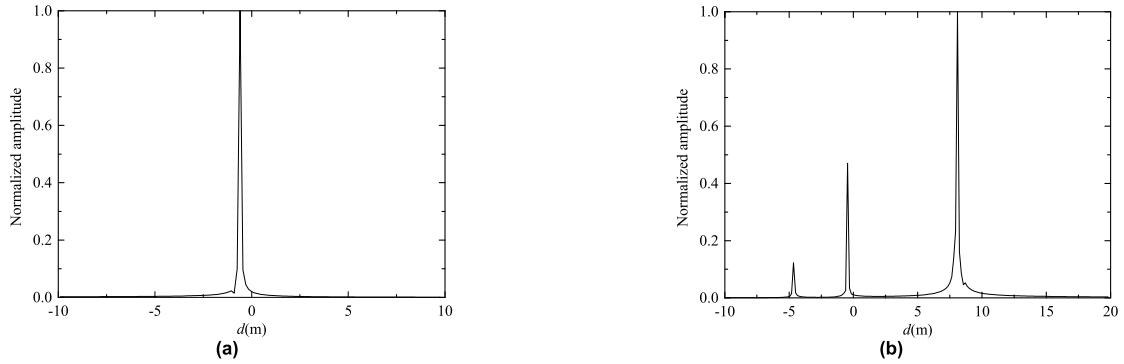

FIGURE 17. The high-resolution range profile of ITTCR, (a) single corner reflector and (b) multiple corner reflectors.

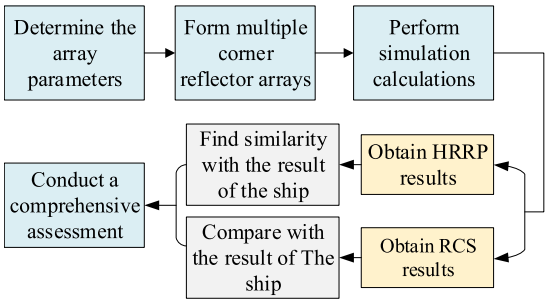

FIGURE 18. The evaluation and optimization flowchart.

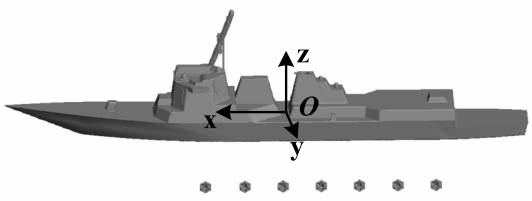

FIGURE 19. Schematic diagram of array arrangement.

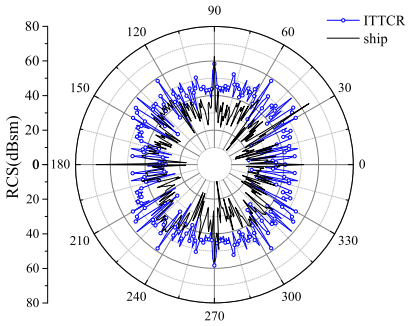

FIGURE 20. The comparison of RCS of ICCTR array and that of ship.

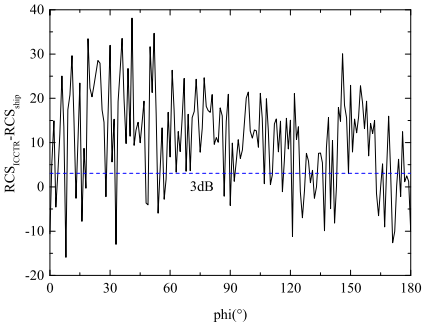

FIGURE 21. The centroid interference intensity results.

A. CALCULATION OF THE RCS AND HRRP RESULTS

The arrangement of corner reflectors needs to consider the simplicity of practical application and the longitudinal size of the ship [21]. Therefore, in our simulations, we assume that they are arranged in a straight line and placed on the side of the ship to achieve better simulation results, see, Fig. 19.

By extracting the number of strong scattering points from different angles of the ship, the scattering points are divided into three levels, high, medium and low, which can be simulated by three different sizes of corner reflectors. According to the position of strong scattering points, the array arrangement is then determined. Moreover, this paper aims to give a jamming evaluation method, so the optimization of the array are not discussed in detail. The corner reflectors with radius of 1 m, 1.5 m, and 2 m are combined to form an array. In the following, this array is used as an example, and its scattering characteristics and range profile are used for evaluation.

The comparison of the RCS results of the array and ship is shown in Fig. 20. In Fig. 21, We then compare the RCS of the two to characterize the centroid jamming effectiveness. Since the model is symmetrical along the axis, we only show the results in the range of $\varphi = 0°$ to $\varphi = 180°$. It can be seen from the figures that, except for individual angles, the RCS of the corner reflector is on average larger than the ship at each angle hence it satisfies the centroid jamming condition.

Fig. 22 shows the range profile of the ship with a zenith angle $\theta = 60°$ and the head-on incidence, i.e., $\varphi = 0°$, with the corresponding relationship between the strong scattering points and the array structures. The range profile variations with the azimuth angle are calculated and shown in Fig. 23. As it is seen, the overall HRRP of the ICCTR array is similar

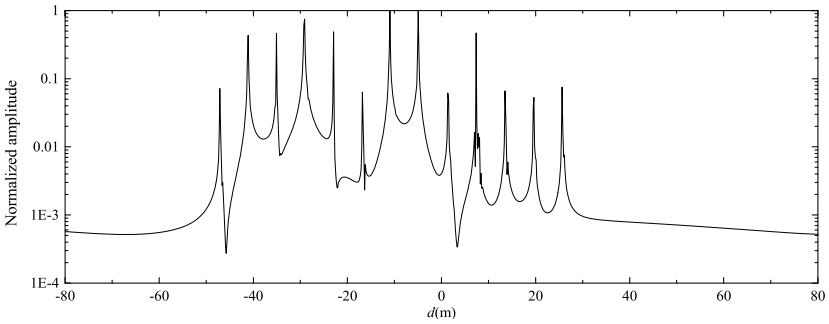

FIGURE 22. The range profile and strong scattering points distribution of ICCTR array.

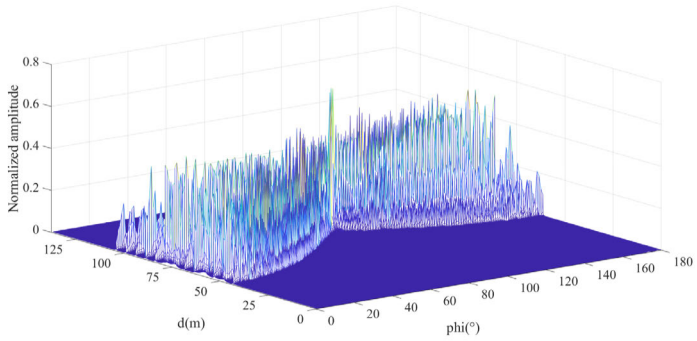

FIGURE 23. The HRRP of ICCTR array at different incident azimuths.

to that of a ship. The results spread over a wide range on the distance axis are more concentrated for sideways incident. Since we only consider three sizes of corner reflectors and fewer fine structures, the peak fluctuations tend to be consistent, and the position coordinates of the strong scattering points do not significantly change with the angle. Nonetheless, the array composed of various sizes is still better than the corner reflectors of the same size.

B. CALCULATION OF SIMILARITY OF HRRP RESULTS

We use the cosine similarity method to calculate the similarity of HRRP between the array and the ship at various angles. We process the range profile results of the corner reflector array at different azimuth angles obtained in the previous section for jamming evaluation. The similarity result is then compared with that of the corner reflector array in the same size and 10 m pitch in the reference [22]. The results are shown in Fig. 24.

The average similarity of the ITTCR array is 0.62. Besides, it can be seen in Fig. 24 that the similarity is higher in the case of head-on and small-angle incidence. In case of the incident from the side, except for the low similarity near the position perpendicular to the ship, other angles maintain a high similarity level. The similarity in the tail incident situation is, however, low, but it also maintains a similarity level greater than 0.55.

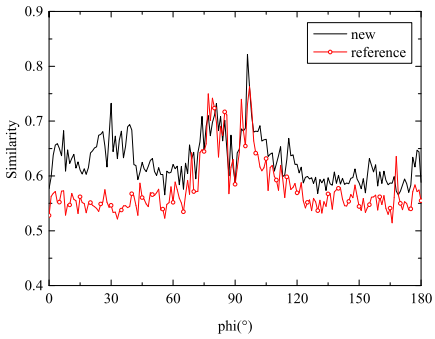

FIGURE 24. The results of HRRP similarity varying with azimuth.

Compared with the similarity results of the same size array in the reference, it is seen that the similarity values of the two are almost the same for lateral incidents. At other incident angles, the similarity of the array mentioned in this paper is higher. It also shows that the cosine similarity method used in this paper is reasonable.

C. PEAK ENVELOPE OF THE HRRP

In the above, when calculating the distance profile similarity, we used the cosine similarity method to investigate the similarity of the result data. To measure the similarity between the jammer and the target, we propose a method to calculate the peak envelope overlapping area of the range profile results. The purpose of this method is to evaluate the similarity of the

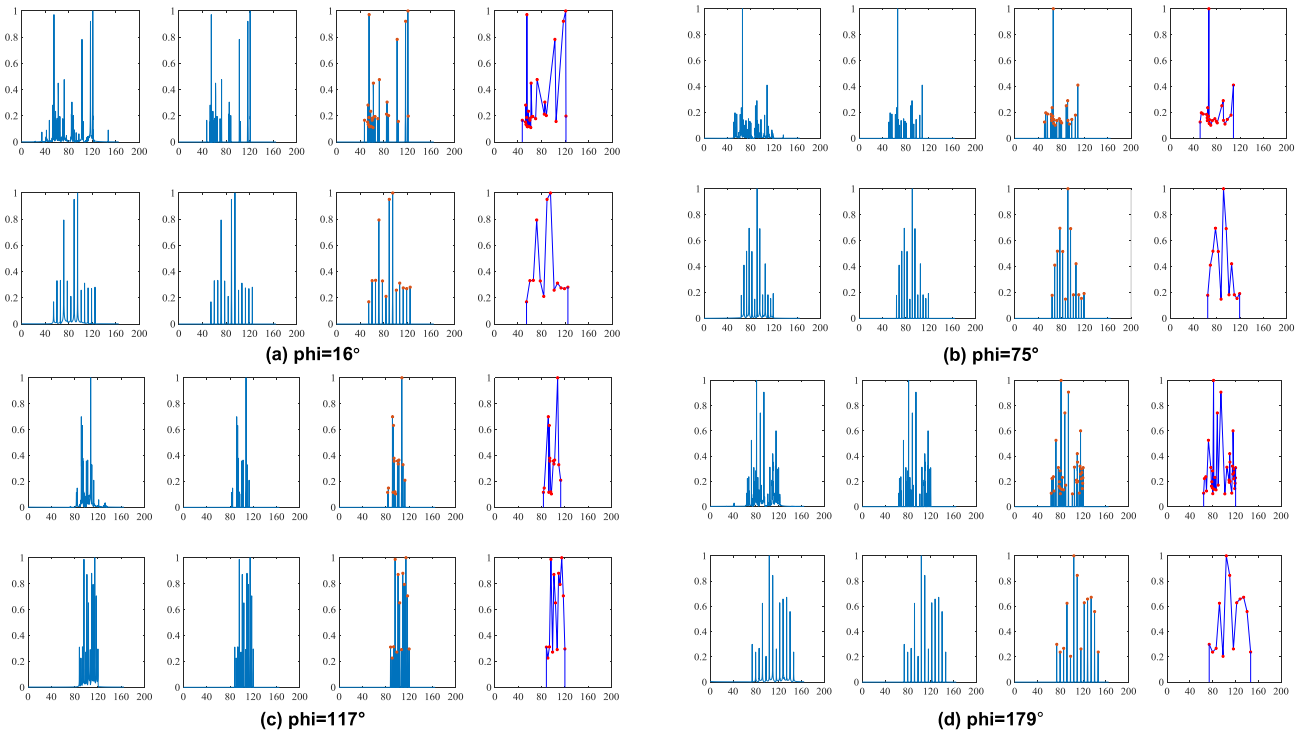

FIGURE 25. The processing steps of range image of ships and corner reflector arrays at different angles.

whole contour of the range profile envelope and is considered as a supplement to the first method.

The processing steps are: 1) remove the small fluctuation points; 2) extract the peak points of the range profile results; 3) connect the peak points to obtain the envelope, and 4) calculate the overlap envelope area between the corner reflector and the ship, and obtain the ratio with the envelope area of the ship.

The abscissa of the four local peak points 16°, 75°, 117°, and 179° separately in the interval $(0°, 45°)$, $(45°, 90°)$, $(90°, 135°)$, $(135°, 180°)$ are selected in the similarity curve of the distance profile. The HRRP results of the array of these angles are compared with the results of the ship.

The processing diagrams of angles 16°, 75°, 117°, and 179° are shown in Fig. 25(a), Fig. 25(b), Fig. 25(c), and Fig. 25(d), respectively. The upper part of each picture is the result of the ship, and the lower part is the result of the ITTCR array. The abscissa of each image is the distance, and the ordinate is the normalized range profile. The ratio of the overlapping area to the envelope area of the ship is 0.4802, 0.4526, 0.4859, and 0.4832, respectively. It is seen that there is a stable similarity in the envelope shape. The similarity also varies with the azimuth angle as shown in Fig. 26. The similarity figures show that the value represented by the overlapping area is lower than that of the previous method at most incident angles. This is because the position of the ship and the corner reflector on the range axis is not the same. The HRRP contour shapes are close to each other, but the result is lower because of the coordinates deviation.

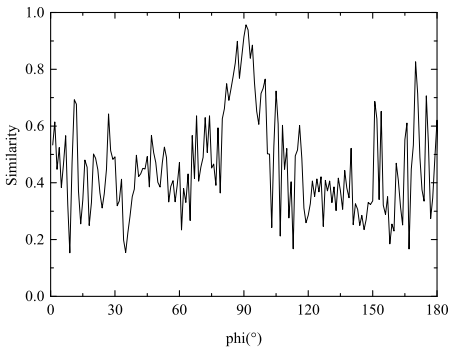

FIGURE 26. The results of HRRP similarity varying with azimuth.

D. EVALUATION SYSTEM AND RESULTS

The comprehensive jamming evaluation in this paper is divided into centroid jamming and deceptive jamming, and the calculation and processing are composed of centroid jamming intensity and range profile similarity. The results are shown in Table 1.

In summary, the jamming effectiveness of the corner reflector array can be assessed using the following three steps. First, it must meet the radar cross-section of the ship and the ship to achieve centroid interference. Second, the similarity of the range profile is measured by the series similarity of the range profile results. Finally, the similarity of the distance profile is also evaluated by using the overlap degree of the profile envelope. This can be summarized in the following expression:

$$J = R_d \times 0.6 + S_1 \times 0.2 + S_2 \times 0.2 \tag{14}$$

TABLE 1. Proportion of evaluation data processing.

Type of jamming	Type of result (weight)	Range of results	Uniform score
Centroid	Difference of RCS (0.6)	<0 dB	0.0
		0~3 dB	0.6
		3~10 dB	0.8
		>10 dB	1.0
Deceptive	Similarity of HRRP (0.4)	0~1	Value = similarity
		0~1	Value = similarity

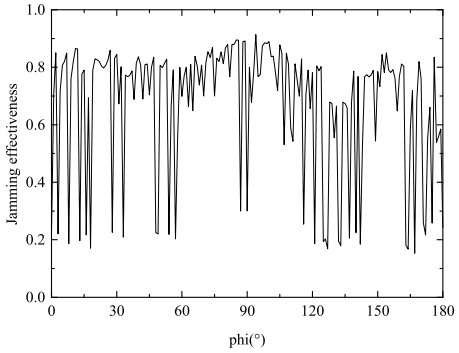

FIGURE 27. The evaluation result of ICCTR array.

where J is the evaluation result, R_d is the score of centroid jamming intensity, and S_1, S_2 are the range profile similarity calculated by the two methods, respectively.

Using (14), the abovementioned three evaluating results are used to analyze the jamming effectiveness of the proposed array, and the results are shown in Fig. 27.

It is seen in Fig. 27 that the corner reflector array calculated in this paper performs efficient jamming at most of the incident angles. The mean value of the data result is 0.6739, which can explain the overall jamming effectiveness of the corner reflector array.

In practical applications, the appropriate weighting of the above three can be applied to measure the jamming effectiveness of the jammer. Based on the scattering data obtained from simulation or testing, the method proposed in this article can be used for jamming performance evaluation.

V. CONCLUSION

The TDSBR method is used to calculate the time-domain electromagnetic scattering characteristics of the ship and corner reflectors. The radar echoes of the targets and jammers under the sea background are simulated by computer programming, and the time-domain echo results are obtained. Using the Fourier transform, the results of the wideband radar scattering and range profile are also derived. Combining simulation and practical results effectively and using the obtained simulation results, the scattering point distribution of the ship is effectively simulated through the arrangement of three different sizes of corner reflector units. We further show that this arrangement is better than a conventional single with the same scattering amplitude corner reflector array. Using the evaluation system which is based on centroid jamming intensity and range profile similarity, the jamming effectiveness of the corner reflector array is also evaluated.

REFERENCES

[1] L. Zhang *et al.*, "Research on current equipment situation and tactical application of ship-born inflatable corner reflector," *J. Ordnance Equip. Eng.*, vol. 39, no. 6, pp. 48–51, Jun. 2018.

[2] G. Chai, M. Yi Lu, and X. M. Chen, "Tactical usage of corner reflector in Navy," *Shipboard Electron. Countermeasure*, vol. 29, no. 5, pp. 11–14, Oct. 2006.

[3] T. Zang, F. F. He, and Q. X. Liu, "Modeling and analysis of adjoint decoy for warship," *Ship Electron. Eng.*, vol. 38, no. 12, pp. 88–92, Dec. 2018.

[4] Z. Y. Zhang and Y. Y. Zhao, "Analysis of electromagnetic scattering characteristic for new type icosahedrons triangular trihedral corner reflectors," *Command Control Simul.*, vol. 40, no. 4, pp. 133–137, Aug. 2018.

[5] W. Yuan, "Passive fake target recognition based on one-dimensional distance image sparse representation," *Telecommun. Eng.*, vol. 58, no. 7, pp. 798–804, Jul. 2018.

[6] X. D. Sun *et al.*, "Survey on the development of towed decoy and its countermeasure technology," *Aerosp. Electron. Warfare*, vol. 31, no. 5, pp. 54–59, May 2015.

[7] J. J. Ding *et al.*, "Analysis of electromagnetic scattering of electrically large objects with time domain shooting and bouncing rays method," *Syst. Eng. Electron.*, vol. 32, no. 9, pp. 1846–1849, Sep. 2010.

[8] S. F. Wang, "Scattering characteristics of time-varying sea surface and its large electrics size targets based on TDSBR," M.S. thesis, School Phys. Optoelectron. Eng., Xidian Univ., Xi'an, China. 2019.

[9] C. Shuai *et al.*, "Simulation on effect of manufacturing deviation of inflatable corner reflector on monostatic RCS," *J. Nanjing Univ. Sci. Technol.*, vol. 43, no. 2, pp. 193–198, Apr. 2019.

[10] C. Li, J. Zhao, J. Yin, G. Zhang, and X. Shan, "Analysis of RCS characteristic of dihedral corner and triangular trihedral corner reflectors," in *Proc. 5th Int. Conf. Comput. Sci. Educ.*, Hefei, China, Aug. 2010, pp. 40–43.

[11] X. J. Shan, J. Y. Yin, and D. L. Yu, "Analysis of artificial corner reflector's radar cross section: A physical optics perspective," *Arabian J. Geosci.*, vol. 2013, no. 6, pp. 2755–2765, May 2012.

[12] W. Han and C. D. Xiao, "Operational method of dilution jamming," *Shipboard Electron. Countermeasure*, vol. 29, no. 5, pp. 47–53, Feb. 2008.

[13] T. Griesser and C. Balanis, "Backscatter analysis of dihedral corner reflectors using physical optics and the physical theory of diffraction," *IEEE Trans. Antennas Propag.*, vol. 35, no. 10, pp. 1137–1147, Oct. 1987.

[14] G. F. Tang *et al.*, "Analysis of corner reflector under naval battlefield," *Electron. Inf. Warfare Technol.*, vol. 30, no. 5, pp. 39–45, May 2015.

[15] J. Zhang, S. L. Hu, and X. M. Fan, "Optimization of the position situation of the air-floating corner reflector based on HRRP and PA," *Tactical Missile Technol.*, vol. 3, no. 17, pp. 105–109, Jul. 2018.

[16] X. Zhou, J. Y. Zhu, W. M. Yu, and T. J. Cui, "Time-domain shooting and bouncing rays method based on beam tracing technique," *IEEE Trans. Antennas Propag.*, vol. 63, no. 9, pp. 4037–4048, Sep. 2015.

[17] X. Zhou, "Hybrid algorithm of electromagnetic transient analysis based on TD-FIT and TDSBR," Ph.D. dissertation, Dept. Inf. Sci. Eng., Southeast Univ., Nanjing, China, 2015.

[18] W. Y. Shuai, X. D. Wang, and A. J. Xue, "Simulation of complete polarized range resolution profile based on FEKO," *J. Projectiles, Rockets, Missiles Guid.*, vol. 34, no. 5, pp. 173–179, Oct. 2014.

[19] J. Fang, Y. J. Li, and K. Zhang, "Modeling and simulation of passive jamming effect assessment based on HLA," *Comput. Simul.*, vol. 25, no. 8, pp. 32–35, Aug. 2008.

[20] W. Han and X. L. Dou, "Analysis on detection of passive centroid jamming effect," *Shipboard Electron. Countermeasure*, vol. 34, no. 6, pp. 48–51, Dec. 2011.

[21] J. Zhang, S. L. Hu, and Q. Yang, "Optimization of position situation of air-floating corner reflectors based on similarity of RCS amplitude characteristic," *J. Nav. Univ. Eng.*, vol. 31, no. 2, pp. 32–36, Apr. 2019.

[22] S. L. Hu, X. M. Fan, and Z. Liu, *Radar Recognition Theory and Method of Corner Reflector Target Based on Ensemble Learning*. Beijing, China: Electronic Industry Press, 2019.

YING LUO received the B.S. degree in electronic information science and technology from Xidian University, in 2014, where she is currently pursuing the M.S. degree in radio physics.

Her research interests include high-frequency calculation of electrically large targets and the jamming effectiveness of passive jammers.

LIXIN GUO (Senior Member, IEEE) received the M.S. degree in radio science from Xidian University, Xi'an, China, in 1993, and the Ph.D. degree in astrometry and celestial mechanics from the Chinese Academy of Sciences, China, in 1999.

From 2001 to 2002, he was a Visiting Scholar with the School of Electrical Engineering and Computer Science, Kyungpook National University, Daegu, South Korea. He has also been a Visiting Professor with the d'Energetique des Systemes et Precedes (LESP), University of Rouen, Mont-Saint-Aignan, France, and with the Faculty of Engineering and Physical Sciences, The University of Manchester, Manchester, U.K. He is currently a Professor and the Head of the School of Physics and Optoelectronic Engineering, Xidian University. He was a recipient of the National Science Fund for Distinguished Young Scholars, in 2012, and a Distinguished Professor of Changjiang Scholars Program, in 2015. He has been a Chief Professor of the Innovative Research Team, Ministry of Science and Technology, China, since 2018. He has authored or coauthored six books and over 300 journal articles. He has been in charge of and undertaken more than 30 projects. His research interests include electromagnetic wave propagation and scattering in complex and random media, computational electromagnetics, inverse scattering, antenna analysis and design.

Prof. Guo was a Fellow of the Chinese Institute of Electronics (CIE) and the Vice President of the Physics Institute of Shaanxi Province, China.

YANCHUN ZUO received the B.E. degree from Xinyang Normal University, Xinyang, China, in 2013, and the M.E. degree from Xidian University, Xi'an, China, in 2014, where he is currently pursuing the D.E. degree in electromagnetic field and microwave technology.

He has published four papers in conference proceedings. His main research interests include electromagnetic scattering modeling and scattering measurements.

WEI LIU (Member, IEEE) received the M.S. degree in mechanical engineering and automation and the Ph.D. degree in radion science from Xidian University, Xi'an, China, in 2003 and 2013, respectively.

He is currently an Associate Professor of Physics and Optoelectronic Engineering with Xidian University. His research interests include electromagnetic wave propagation and scattering in complex and random media, and computational electromagnetics.